# A comparative study of the atomic structures of Ge-doped $As_4S_3$ and $P_4Se_3$ molecular glasses

B. Kalkan[a,b,*], C. J. Benmore[c], B.G. Aitken[d], S. Sen[e] and S. M. Clark[f]

[a] *Department of Physics Engineering, Hacettepe University, Beytepe 06800, Ankara, TURKEY.*

[b] *Advanced Light Source, Lawrence Berkeley Laboratory, Berkeley, California 20015, USA.*

[c] *X-ray Science Division, Argonne National Laboratory, Argonne, IL 60439, USA.*

[d] *Science and Technology Division, Corning Incorporated, Corning, NY 14831, USA.*

[e] *Department of Materials Science & Engineering, University of California–Davis, Davis, California 95616, USA.*

[f] *Department of Earth and Planetary Sciences, Macquarie University, North Ryde, 2019 NSW, Australia.*

The structures of pseudo-binary P-Se and As-S glasses with compositions close to the $P_4Se_3$ and $As_4S_3$ stoichiometry with a few atom %Ge doping were determined using Monte Carlo simulations constrained by density and x-ray scattering measurements. We find that these glasses consist predominantly of $P_4Se_3$ and $As_4S_3$ molecules, presumably held together by van der Waals forces. The Ge doping results in some important differences between the two glasses. The P-Se glass displays significantly higher intermolecular connectivity via P-Se-Ge linkages, consistent with the significantly higher glass transition temperature and lower fragility of this liquid compared to its As-S counterpart. We also speculate that a consequence of this difference in the intermolecular connectivity would be to delay any pressure-induced conversion from a molecular to a network structure for the Ge doped P-Se glass compared to the Ge-doped As-S glass.

*Keywords: Chalcogenide glasses, short and intermediate range order, Monte Carlo, molecular structure, topology.*

## 1. Introduction

Chalcogenide glasses are important materials with promising applications in the areas of infrared photonics, memory and sensing technologies [1-5]. The high compositional flexibility of these materials provides the potential to finely tune their optical, electronic and thermomechanical properties by selection of an appropriate stoichiometry [6, 7] although this requires a good understanding of their atomic structure and its relation to their physical properties. The structure of binary phosphorus selenide and arsenic sulfide glasses has been studied extensively due to their large glass-forming region and interesting physical properties [8-14]. In particular, the structure of molecular glasses in these systems has been a matter of great and continuous interest in the literature [10, 11, 15-19].

The bulk glass formation region in the $As_xS_{1-x}$ system starts at about x=0.05 and ends at about x=0.46 [20]. In the sulfur rich region, the structure consists of sulfur chains cross linked by $AsS_3$ pyramids together with a significant number of $S_8$ rings [21]. With increasing As content, the concentration of $S_8$ rings decreases and a network of corner-sharing $AsS_{3/2}$ pyramids forms at the stoichiometric composition $As_2S_3$. Further increase in As content results in the formation of $As_4S_4$ molecules together with homopolar As-As bonds [22, 23]. Pseudo-binary glasses in the Ge-As-S system along the join $GeS_2$-$As_4S_3$ with compositions near $Ge_3As_{52}S_{45}$ are composed predominantly of $As_4S_3$ molecules held together by van der Waals forces [17]. The $As_4S_3$ molecules are topologically similar to $P_4Se_3$ molecules with a cage-like structure [15]. These molecules consist of a three-membered $As_3$ (or $P_3$) ring bonded to a $AsS_3$ (or $PSe_3$) pyramid with each S (or Se) atom bonded to an As (or P) atom in the $As_3$ (or $P_3$) ring and the apical As (or P) atom pointing away from the $As_3$ (or $P_3$) ring.

Bulk glass formation in the $P_xSe_{1-x}$ system occurs over a wide range of compositions $0<x<0.80$, except for a narrow window $0.52<x<0.60$ centered at $x=0.57$ corresponding to the $P_4Se_3$ stoichiometry [13]. Previously, the intermediate- and short-range structures of $P_xSe_{1-x}$ glasses in two glass regions, $x$=0.025–0.54 and 0.64–0.84 have been reported [14]. Results indicate 3-coordinated P is the dominant structure at ~ $x$=0.05. At approximately $x$=0.25, $Se_{2/2}P$-$PSe_{2/2}$ units start to appear and remain stable up to $x$=0.54, the end of the Se-rich region [14]. Moreover, 4-coordinated P with P=Se bonds have also been observed up to ~ $x$=0.3. Above $x$=0.3, $P_4Se_3$ molecules with a cage-like structure start to appear and increase up to $x$=0.54 [10, 14]. In

phosphorus rich stoichiometries, the dominant structural motifs are the $P_4Se_3$ molecule and a red phosphorus like network (dominating at the highest P content) [14]. The P-Se and P-P bond lengths are found to increase with increasing P concentration. However, the structure of $P_xSe_{1-x}$ glass in the $0.52<x<0.60$ window cannot be stabilized without doping with Ge.

In spite of the structural similarities between the molecular glasses in the As-S and P-Se systems, the corresponding parent liquids were reported to have quite different temperature dependencies of their viscosities near the glass transition [11, 18]. The fragility index $m$ is a measure of the rate of change in viscosity $\eta(T)$ with temperature near and above the glass transition temperature $T_g$, and is defined as $m = \left.\frac{dlog\eta(T)}{d(T_g/T)}\right|_{T=T_g}$. The fragility $m$ of the molecular As-S and P-Se liquids were reported to be 102 and 46 respectively. Here, we present a structural investigation of a P-Se glass with a P:Se ratio close to $P_4Se_3$ stabilized by the addition of 2.8 atom %Ge. The results are compared with those obtained for a molecular pseudo-binary As-S glass doped with Ge with composition near $Ge_3As_{52}S_{45}$ that is expected to be composed predominantly of $As_4S_3$ molecules which are topologically similar to $P_4Se_3$ molecules with a common cage structure. We demonstrate that the two glasses, in spite of their predominantly molecular character, differ significantly in their intermediate-range structure, particularly the inter-molecular connectivity, which can explain the differences in the fragility of their parent liquids.

## 2. Experimental

Ge doped As-S and P-Se glasses were synthesized by melting mixtures of constituent elements (≥99.999% purity) in evacuated ($10^{-6}$ Torr) and sealed silica ampules at temperatures of 873 -1073 K for at least 24 h in a rocking furnace. The ampules were subsequently quenched in cold water. Chemical compositions of the samples were determined using electron probe microanalysis to be $Ge_{2.8}P_{57.7}Se_{39.5}$ (GPS) and $Ge_{2.5}As_{51.25}S_{46.25}$ (GAS). X-ray diffraction data were collected on beamline 6-ID-D of the Advanced Photon Source. A single x-ray wavelength was selected using a Si(311) bent Laue monochromator. Angle-dispersive diffraction data were collected using an incident photon energy of 100 keV, allowing a maximum Q range of up to ~20 $Å^{-1}$. The unfocused beam size is 1x1 $mm^2$. A Perkin-Elmer large area detector was used to collect the diffraction images. The sample to detector distance and the detector tilt angles were determined using powder diffraction from a $LaB_6$ standard. The x-ray beam was 99% horizontally polarized and all

geometric and polarization corrections were made during the angular integration using the FIT2D software package [24].

The Empirical Potential Structure Refinement (EPSR) method was used to determine the atomic structures of GPS and GAS glasses at ambient conditions [25, 26]. For each simulation 56 Ge (or 50 Ge), 1154 P (or 1025 As) and 790 Se (or 925 S) atoms were mixed in a cubic simulation box with a volume constrained by the experimentally determined glass densities (Table 1). The minimum approach distances are listed in Table 1 and the values used for the Lennard-Jones potential well depth and range parameters are listed in Table 2.

## 3. Results and Discussion

*3.1. Structure factor and the first sharp diffraction peak.* The experimentally determined x-ray total structure factors, S(Q), for GAS and GPS are compared with those calculated from our EPSR simulations in Fig. 1. The S(Q) curves are characterized by an intense first sharp diffraction peak (FSDP) at about 1.18 $Å^{-1}$ for both GAS and GPS. The FSDP indicates intermediate range order at length scales of about 5.4 Å presumably resulting from the strong intermolecular correlations in these glasses. The FSDP for GAS is more intense than that for GPS implying stronger intermediate range order compared to GAS. Given the very similar molar volumes of GAS (16.43 $cm^3$) and GPS (16.53 $cm^3$) this is most probably due to differences in inter-molecular orientational correlation between the two materials, resulting from differences in connectivity (see below) [15]. The FSDP position, $Q_{FSDP}$, has been shown to be related to the inter-molecular packing fraction of cages in P-S glasses [14]. If we assume the volume of a cage molecule to be approximately spherical it follows that $V_p=\pi\sigma^3/6$, where sigma represents the sphere diameter. From the relation $2\pi/Q_{FSDP}$ we find $\sigma$=5.33 Å for GPS, corresponding to a cage volume of $V_p$=79.3 $Å^3$. Compared to the volume of a $P_4Se_3$ or $As_4S_3$ cage calculated using the bulk molecular number density for GPS ($V_p$=200 $Å^3$), this yields an inter-molecular packing fraction of 40%. A similar calculation for GAS gives an inter-molecular packing fraction of 41%. This is consistent with a void fraction calculation of 62% for both GPS and GAS from our EPSR atomistic models (see supplementary information Fig. S1), which is the volume of unoccupied space obtained if we fill the simulation box with small spherical voids of radii ~1.4 Å, chosen to be just over half the shortest bond length. The partial structure factors (PSFs) obtained from EPSR simulations (Fig. 2) indicate that the FSDP for GPS has contributions from P-Se, P-P, and Se-Se correlations whereas

GAS is dominated by just the As-As interactions. This means that there are repetitive correlations between these atoms on a length scale of ~5.33 Å, suggesting quite different molecular interactions in two cases, and stronger molecular connectivity in GPS compared to GAS. The chemical and topological ordering in an amorphous structure is characterized by the principal peak (or second sharp diffraction peak) and third peak, respectively. A more intense principal peak in the S(Q) of GPS indicates that chemical ordering dominates at the extended range length scale, while the third peaks exhibit relatively small variations and occur near $Q = 5\pi/2r$, where r is the mean nearest-neighbor distance. The PSFs reveal that the principal peak arises from S(Se)-S(Se), As(P)-S(Se), and As(P)-As(P) correlations. Ge-S(Se) anti-correlations cause a partial cancellation of the principle peak.

*3.2. EPSR simulation.*

*3.2.1. Pair distribution function and coordination environments.* The total pair distribution functions (PDFs) determined from the EPSR simulations are shown in Fig. 3, and compared with those calculated from the experimental data. Partial pair distribution functions (pPDFs) determined from the EPSR simulations are contained in Fig. 4. A comparison between the PDFs and pPDFs shows that the first peak in the total PDFs in the region 2.0–2.9 Å corresponds to a combination of P-P (or As-As), P-Se (or As-S), and Ge−Se (or Ge-S) nearest-neighbor correlations. One of these is from intra-tetrahedral Ge-Se and four coordinated Ge-S correlations and the others are due to P-Se (or As-S) and P-P (or As-As) correlations in $P_4Se_3$ or $As_4S_3$ molecules. The peak positioned at about 3.7 Å in the PDFs can be correlated with *i*) intra-tetrahedral Se−Se (or S-S) correlations in $GeSe_4$ or $GeS_4$ units and *ii*) the distance between apical and basal P (or As) atoms in $P_4Se_3$ or $As_4S_3$ molecules. The two peaks located at about 5.85 Å and at about 6.95 Å in the PDF correspond to intermolecular correlations in the glass structure, and dominated by P-P (or As-As), P-Se (or As-S), and Se−Se interactions (insets of Fig. 4b, 4c, and 4d). No Ge-Ge and Ge-P (or Ge-As) correlations are observed in the pPDFs.

The nearest-neighbor coordination numbers $n_{GeSe(S)}$, $n_{PP(AsAs)}$, and $n_{P(As)Se(S)}$, total coordination numbers around P (or As) and Se (or S), and the average first shell coordination numbers calculated from the EPSR simulations are shown in Fig. 5. According to the 8-N rule, the coordination numbers of Ge, Se (or S) and P (or As) atoms are expected to be 4, 2 and 3, respectively, which would lead to an average first shell coordination number, $n_{average}$ of 2.63 for both GPS and GAS

compositions. Our data indicates that $n_{average}$ for the GPS and GAS glasses are about 2.64 and 2.68, respectively. The average values of $n_{GeSe(S)}$ for GAS and GPS, calculated using only first shell Ge-Se or Ge-S correlations, are 3.45 and 3.66 respectively. Total coordination numbers around P and As atoms were calculated using first shell P-P and P-Se, or As-As and As-S correlations, and found to be 3.10 and 3.20 respectively. Similarly, total coordination numbers around Se and S atoms were calculated using first shell Se-Ge and Se-P, or S-Ge and S-As correlations to give 2.10 and 1.96 respectively. The integration of the second peak in $g_{SeSe(SS)}(r)$ yields a second shell Se-Se (or S-S) coordination number of about 8.8 and 5.2 for GAS and GPS, respectively.

*3.2.2. Bond angle distributions.* The bond angle distribution functions for GAS and GPS are shown in Fig. 6. A schematic representation of structural motifs in GAS and GPS which give rise to these peaks are also shown in Fig. 7. The maximum at about 109° in the Se−Ge−Se distribution is very close to the tetrahedral angle of 109.5° in a perfect tetrahedron and indicates that there is close to 4-fold Se coordination around Ge. In contrast to the Se−Ge−Se distribution in $GeSe_4$, the S−Ge−S bond angle in $GeS_4$ is 93° which is in good agreement with the previous results observed in germanium sulfide, $GeS_n$, structures [27-29]. The large distribution and center positions of the bond angle distributions are the signatures of an imperfect tetrahedral structure and of the structural disorder of a glassy sample. The Ge-Se-Ge bond distribution is also characterized by a broad peak centered at about 112° which may be associated with corner-sharing $GeSe_4$ units [30]. The peak at about 99° in the Ge-S-Ge bond angle distribution can be associated with the connection of distorted $GeS_4$ units via corner sharing (Fig. 7) which we find explicitly in our simulation results (Figs 8a and 8b). This reflects structural insights about the linkages of $GeSe_4$ (or $GeS_4$) structural units (random/nonrandom distribution) among $P_4Se_3$ (or $As_4S_3$) cage molecules. Of particular interest is the P−Se−Ge bond angle distribution that may characterize P-Se bonding between $P_4Se_3$ cage molecules and $GeSe_4$ tetrahedra. The As−S−Ge bond angle distributions are consistent with a scenario where some apical As atoms in the $As_4S_3$ molecules have been replaced with Ge atoms which are connected to edge-shared $GeS_4$ tetrahedra and $AsS_3$ pyramids to give $GeS_3As_3$ molecules. The broad peak at 95° would then correspond to the intra-molecular angle in the $GeS_3As_3$ molecules [27- 30]. However, no corresponding P−Se−Ge distributions are found in the GPS bond angle distributions indicating that Ge does not replace the apical P atom in the $P_4Se_3$ cage molecules. This result supports the existence of rigid intermolecular $GeSe_4$ (or $GeS_4$) structural units in the structure. The Se−Se−Se bond angle distribution is characterized by a sharp

peak at about 58° and the S-S-S bond angle distribution by a corresponding strong peak at about 56°. These correspond to the intra-tetrahedral Se-Se-Se angle and S-S-S angle on $GeSe_4$ and $GeS_4$ tetrahedra surfaces respectively. There is also a broad peak ranging from 100° to 130° with a maximum at about 112° in both bond angle distributions which is due to inter-tetrahedral unit correlations. The Se−P−Se bond distribution has a main peak at about 100° arising from $P_4Se_3$ molecules where the apical P atom is linked to three Se atoms giving $PSe_3$ pyramids [5, 15]. As for $P_4Se_3$ the S−As−S bond angle in the $As_4S_3$ molecules is characterized by a peak at about 102° [15, 16]. The P-Se-P and As-S-As bond angle distributions are characterized by two main peaks centered at about 102 °(or 92°) and 60° (or 52°) respectively. The peak centered at about 100° (or 92°) arises from the linkage of apical P (or As) atoms to the basal $P_3$ (or $As_3$) plane via P-Se (or As-S) bonds. The sharp peak at about 60° (or 52°) in P-Se-P (or As-S-As) is also present in the crystal structure of $P_4Se_3$ (or $As_4S_3$) and can be attributed to the inter-molecular angle between a bonded P (or As) and Se (or S) and a non-bonding P (or As) on the next molecule [5, 9, 10, 11, 15, 16]. The peak at about 52° in the As-S-As bond angle distribution may also arise from bonding between $AsS_3$, edge shared with a $GeS_4$ polyhedron and an adjacent $AsS_3$ through an As-S-As bridge (Fig. 7). The maximum at ∼60° in the P-P-P (or As-As-As) distribution is close to the internal angles of the intra-molecular basal $P_3$ (or $As_3$) planes and may also correspond to amorphous red Phosphorus type $P_3$ triangles and $P_4$ pyramidal subunit structures (Figs. 7 and 8c). The broad peak ranging from 80° to 130° with the maxima at about 98° and 107° in the P-P-P and As-As-As distributions respectively may arise from the linkage of two $P_4Se_3$ (or $As_4S_3$) molecules by two supplementary P (or As) atoms as represented in Fig. 7. Similar inter- and intra- molecular angles are also observed in the S-As-As and Se-P-P bond angle distributions at about 61° (or 60°) and 97° or (98°), respectively.

*3.2.3. Partial pair distribution functions.* For the GAS and GPS glasses Ge-S (or Ge-Se), As-S (or P-Se) and As-As (or P-P) pPDFs display strong peaks at about 2.33 Å and 2.12 Å, 2.48 Å and 2.30 Å and 2.23 Å and 2.30 Å. These correspond to bond lengths in the short-range ordering (Fig. 4). The radius of the first- and second-coordination shells Ge-S (or Ge-Se) ($r_1$=2.33 Å (or 2.12 Å)) and S-S (or Se-Se) ($r_2$=3.83 Å (or 3.54 Å)) give $r_1/r_2$ ratios of 0.61 and 0.60. These taken together with the related bond angle distributions and coordination numbers indicate the presence of a tetrahedral bond structure inside the two glasses. The P-Se-P (or As-S-As), Se−P−Se (or S-As-S), and Se-P-P (or S-As-As) bond angle distributions and the lack of S-S (or Se-Se) bonding

in the first shell indicate the presence of a molecular structure. These values obtained in the present study are in good agreement with the inter-molecular angles and bond lengths of $P_4Se_3$ (or $As_4S_3$) cage-like structures. A schematic representation of the atomic arrangements in the short- and intermediate- range length scales for each system is shown in Fig. 9.

*3.3. Implications for physical properties.* The Ge doping results in some important differences in intermolecular connectivity between the two glasses that offer an explanation for the differences in their physical properties. In the P-Se glass a significant fraction of the $P_4Se_3$ molecules are connected by single and corner-shared $GeSe_4$ tetrahedra via P-Se-Ge linkages. In the As-S glass there is little inter-molecular connectivity, except that some of the $As_4S_3$ molecules are linked by two supplementary As atoms (Fig. 7). The $GeS_4$ polyhedral units are linked to adjacent $AsS_3$ pyramids through Ge-S-As bridges, but do not take part in inter-molecular connectivity. These structural differences between the Ge doped P-Se and As-S glasses lead us to conclude that the former has higher inter-molecular connectivity. This connectivity may result in a network-like structure and a loss of inter-molecular orientational correlation, which is indeed in agreement with the observation that the GPS glass is characterized by a lower intensity of the FSDP compared to the GAS glass. Moreover, this difference in the inter-molecular connectivity can explain the previously reported results of the glass transition and viscosity measurements performed on the $Ge_3As_{52}S_{45}$ and $P_5Se_3$ liquids, which provided the glass transition temperature $T_g$ of these liquids to be ~ 312K and 468 K, and the corresponding fragility indices $m$ to be ~ 102 and 46, respectively [11, 17, 18]. The high fragility and low $T_g$ of the $Ge_3As_{52}S_{45}$ liquid is consistent with its less connected structure, which allows for facile temperature dependent exploration of alternative configurations in the energy landscape of the supercooled liquid. It is also crucial to understand how these differences in intermolecular connectivity affect the mechanical properties (such as compressibility) and structural stability under pressure with increase in density [31, 32] since these properties are sensitive to both short-range and medium-range ordering. Moreover, polyamorphic phase transitions are often associated with a distinct change in the structure of a glass from strong to fragile with increase of density [31, 32]. Recently, we have reported the observation of a pressure-induced polyamorphic transition between a low-density molecular structure and a high-density network structure near ~2 GPa in glassy $Ge_{2.5}As_{51.25}S_{46.25}$ at ambient temperature [33-35]. For the GPS glass, the structural results presented here indicate a more connected intermolecular structure and it is tempting to speculate that consequently higher pressures would be required to

induce any conversion from a molecular to a network structure compared to GAS glass. Experimental confirmation of this hypothesis is currently the subject of an ongoing investigation.

## 4. Conclusion

We have studied the short- and intermediate- range order in the atomic structure of Ge-doped pseudo-binary P-Se and As-S glasses at room temperature and ambient pressure, using x-ray scattering supplemented with 3D atomistic modelling obtained from Monte-Carlo simulations. The combined results strongly suggest that the structure of GAS and GPS glasses predominantly consists of $P_4Se_3$ and $As_4S_3$ molecules. Doping with Ge results in the formation of P-Se-Ge linkages between the $P_4Se_3$ molecules via single or multiple corner-shared $GeSe_4$ tetrahedra. While for the GAS glass, the results suggest little connectivity between the $As_4S_3$ molecules and the Ge doping results in corner sharing $GeS_4$ tetrahedra forming small pieces of a $GeS_2$ network with some non-bridging S terminating these pieces of the network. The analyses of the partial structure factors obtained from the EPSR simulations reveal different contributions to the FSDP for GAS and GPS suggesting quite different molecular interactions in the two cases, and stronger molecular connectivity in GPS compared to GAS. Such structural differences are consistent with the $T_g$ of these glasses and the fragility of their parent liquids.


## Acknowledgements

The Advance Photon Source is supported by the U.S. Department of Energy under Contract No. DE-AC02-06CH11357. B.K. acknowledges financial support from Scientific Research Projects Coordination Unit, Hacettepe University on project number FBI-2016-9682. The work at UCD was supported by an NSF grant DMR-1505185.


## References


[1] A. Zakery, S. R. Elliott, **Optical Properties and Applications of Chalcogenide Glasses: A Review**. *J. Non-Cryst. Solids* 330, 1−12 (2003).

[2] K. Shimakawa, A. V. Kolobov, S. R. Elliott, **Photoinduced Effects and Metastability in Amorphous Semiconductors and Insulators**. *Adv. Phys.* 44, 475−588 (1995).

[3] M. Wuttig, N. Yamada, **Phase-change materials for rewriteable data storage**, *Nature Matt.* 6, 824-832 (2007).

[4] L. Li, H. Lin, S. Qiao, Y. Zou, S. Danto, K. Richardson, J. D. Musgraves, N. Lu and J. Hu, **Integrated flexible chalcogenide glass photonic devices**, *Nature Photonics* 8, 643-649 (2014).

[5] S. Cui, R. Chahal, Y. Shpotyuk, C. Boussard, J. Lucas, F. Charpentier, H. Tariel, O. Loreal, V. Nazabal, O. Sire, V. Monbet, Z. Yang, P. Lucas, and B. Bureau, **Selenide and telluride glasses for mid-infrared bio-sensing**, *Proc. SPIE* 8938, 893805/1-9 (2014).

[6] Y. Yang, Z. Yang, P. Lucas, Y. Wang, Z. Yang, A. Yang, B. Zhang, H. Tao, **Composition dependence of physical and optical properties in Ge-As-S chalcogenide glasses**. *J. Non-Cryst. Solids* 440, 38–42 (2016).

[7] E. Zhu, X. Zhao, J. Wang, C. Lin, **Compositional dependence of physical and structural properties in $(Ge_{1-x}Ga_x)S_2$ chalcogenide glasses**. *J. Non-Cryst. Solids* 489, 45-49 (2018).

[8] D. J. Verrall, S. R. Elliot, **Structure of phosphorus selenide glasses.** *J. Non-Cryst. Solids* 114, 34 (1989).

[9] P. Chen, C. Holbrook, P. Boolchand, D. G. Georgiev, K. A. Jackson, and M. Micoulaut, **Intermediate phase, network demixing, boson and floppy modes, and compositional trends in glass transition temperatures of binary $As_xS_{1-x}$ system.** *Phys. Rev. B* 78, 224208 (2008).

[10] D. J. Verrall, S. R. Elliot, **Experimental Evidence for an Inorganic Molecular Glass.** *Phys. Rev. Lett.* 61, 974 (1988).

[11] E. L. Gjersing, S. Sen, P. Yu, B. G. Aitken, **Anomalously large decoupling of rotational and shear relaxation in a molecular glass.** *Phys. Rev. B* 76, 214202 (2007).

[12] C. Y. Yang, M. A. Paesler, and D. E. Sayers, **Chemical order in the glassy $As_xS_{1-x}$ system: An x-ray-absorption spectroscopy study**. *Phys. Rev. B* 39, 10342 (1989).

[13] D. G. Georgiev, M. Mitkova, P. Boolchand, G. Brunklaus, H. Eckert, and M. Micoulaut, **Molecular structure, glass transition temperature variation, agglomeration theory, and network connectivity of binary P-Se glasses**. *Phys. Rev. B* 64, 134204 (2001).

[14] A. Bytchkov, M. Miloshova, E. Bychkov, S. Kohara, L. Hennet, and D. L. Price, **Intermediate- and short-range order in phosphorus-selenium glasses**. *Phys. Rev. B* 83, 144201 (2011).

[15] E.L. Gjersing, S. Sen, B.G. Aitken, **Molecular dynamics in supercooled P-Se liquids near the glass transition: results from $^{31}P$ NMR spectroscopy**. *J. Phys. Chem. B* 115, 2857-2863 (2011).

[16] S. Soyer-Uzun, S. Sen, B. G. Aitken, **Network vs molecular structural characteristics of Ge-doped arsenic sulfide glasses: a combined neutron/x-ray diffraction, extended x-ray absorption fine structure, and raman spectroscopic study.** *J. Phys. Chem.* C 113, 6231-6242 (2009).

[17] B. G. Aitken, **GeAs sulfide glasses with unusually low network connectivity.** *Journal of Non-Crystalline Solids* 345, 1-6 (2004).

[18] D. C. Kaseman, O. Gulbiten, B. G. Aitken, and S. Sen, **Isotropic rotation vs. shear relaxation in supercooled liquids with globular cage molecules.** *J. Chem. Phys.* 144, 174501 (2016).

[19] A. C. Wright, B. G. Aitken, G. Cuello, R. Haworth, R. N. Sinclair, J. R. Stewart, J. W. Taylor, **Neutron studies of an inorganic plastic glass.** *J. Non-Cryst. Solids* 357, 2502-2510 (2011).

[20] Z.U. Borisova, **Glassy Semiconductors**, Plenum Press, (1981).

[21] P. Bonazzi, L. Bindi, **A crystallographic review of arsenic sulfides: effects of chemical variations and changes induced by exposure to light**. *Z. Kristallogr.* 223, 132–147 (2008).

[22] C. Y. Yang, M. A. Paesler, and D. E. Sayers, **Chemical order in the glassy $As_xS_{1-x}$ system: An x-ray-absorption spectroscopy study**. *Phys. Rev. B* 39, 10342 (1989).

[23] D. G. Georgiev, P. Boolchand, K. A. Jackson, **Intrinsic nanoscale phase separation of bulk $As_2S_3$ glass**. *Philosophical Magazine* 83:25, 2941-2953 (2003).

[24] A. P. Hammersley, , S. O. Svensson, , M. Hanfland, A. N. Fitch, D. Hausermann, **Two-dimensional detector software: from real detector to idealized image or two-theta scan**. *High Pressure Research* 14, 235 (1996).

[25] Soper, A. K. **Partial structure factors from disordered materials diffraction data: An approach using empirical potential structure refinement.** *Phys. Rev. B* 72, 104204/1−104204/12 (2005).

[26] J.M. Zaug, A.K. Soper and S.M. Clark, **The pressure-dependent structures of amorphous red phosphorus and the origin of the first sharp diffraction peak**, *Nature Materials* 7, 890-899 (2008).

[27] J Akola, B Beuneu, R O Jones, P Jóvári, I Kaban, J Kolář, I Voleská and T Wágner, **Structure of amorphous Ag/Ge/S alloys: Experimentally constrained density functional study**. *Journal of Physics Condensed Matter* 27(48), 485304 (2015).

[28] S. Blaineau, P. Jund, D. A. Drabold, **Physical properties of a $GeS_2$ glass using approximate *ab initio* molecular Dynamics.** *Phys. Rev. B* 67, 094204 (2003).

[29] K. Itoh, **Structural study of $GeS_2$ glass: Reverse Monte Carlo modelling for edge-sharing tetrahedral network**. *Journal of Physics and Chemistry of Solids* 103, 109–115 (2017).

[30] B. Kalkan, R. P. Dias, C.-S. Yoo, S. M. Clark, S. Sen, **Polyamorphism and Pressure Induced Metallization at the rigidity percolation threshold in densified $GeSe_4$ glass**. *J. Phys. Chem. C* 118 (10), 5110-5121 (2014).

[31] I. Saika-Voivod, P. H. Poole, and F. Sciortino, **Fragile-to-strong transition and polyamorphism in the energy landscape of liquid silica**. *Nature* (London) 412, 514 (2001).

[32] P. H. Poole, T. Grande, C. A. Angell, and P. F. McMillan, **Polymorphic phase transitions in liquids and glasses.** *Science* 275, 322 (1997).

[33] S. Sen, S. Gaudio, B.G. Aitken, C. E. Lesher, **Observation of a pressure-induced first-order polyamorphic transition in a chalcogenide glass at ambient temperature.** *Phys. Rev. Lett.* 97, 025504 (2006).

[34] S. Soyer-Uzun, S.J. Gaudio, S. Sen, Q. Mei, C. Benmore, C.A. Tulk, J. Xu, B.G. Aitken, **In situ high-pressure x-ray diffraction study of densification of a molecular chalcogenide glass.** *J. Phys. and Chem. of Solids* 69, 2336-2340 (2008).

[35] B. Kalkan, C. Sonneville, C. Martinet, B. Champagnon, B.G. Aitken, S.M. Clark, S. Sen, **Hysteretically reversible phase transition in a molecular glass.** *J. Chem. Phys.* 137, 224503 (2012).

**Figures**

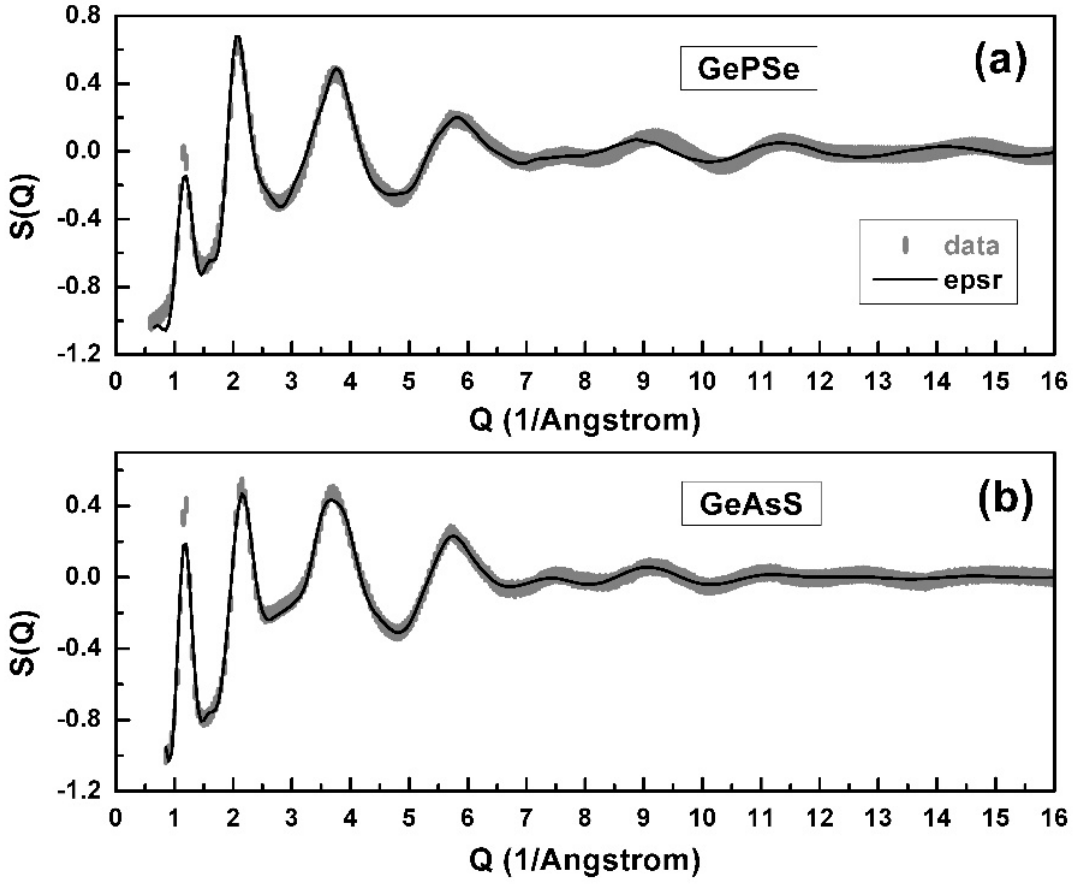


Figure 1. Total structure factors, S(Q), for (a) GPS and (b) GAS calculated from our X-ray scattering data (thick gray bars) compared to values given by our EPSR simulations.

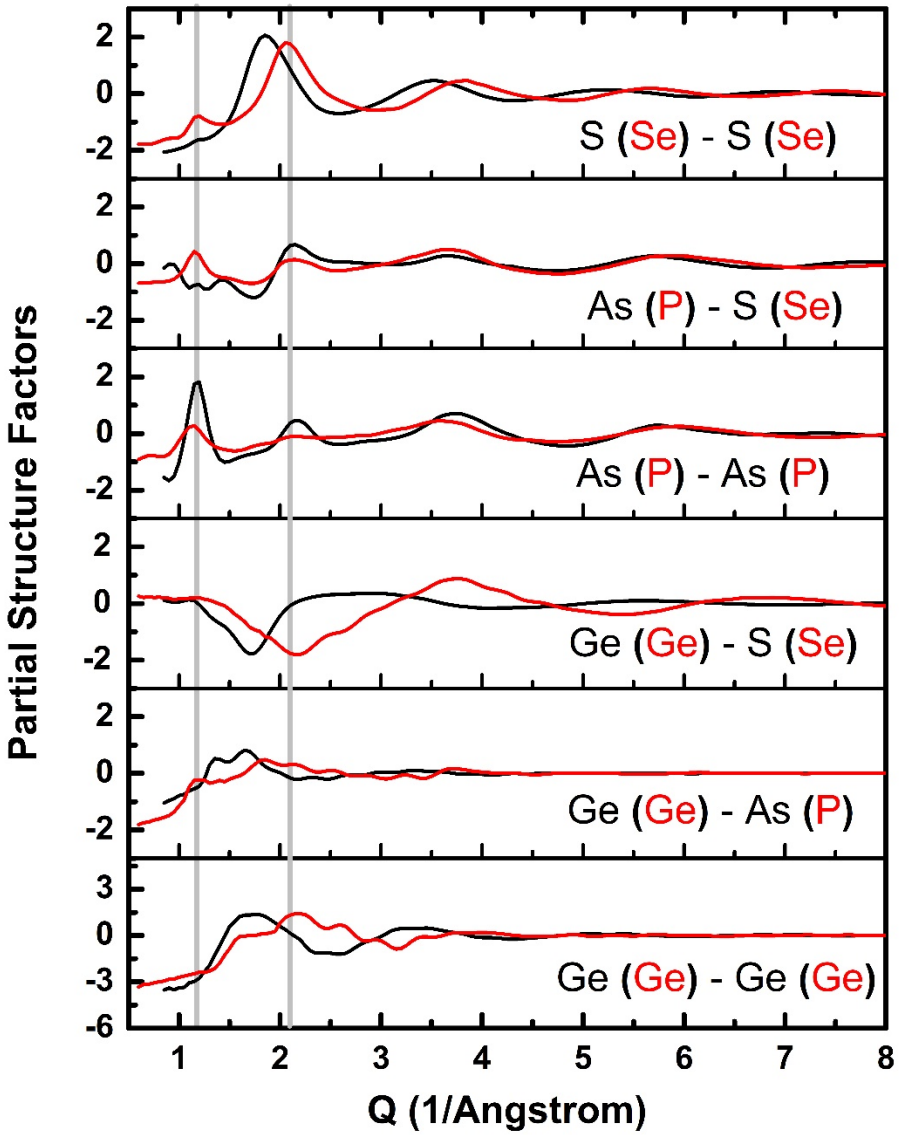


Figure 2. Partial structure factors for GPS and GAS calculated from EPSR simulations. The gray vertical lines indicate the positions of FSDP and principal peak in total structure factor.

,

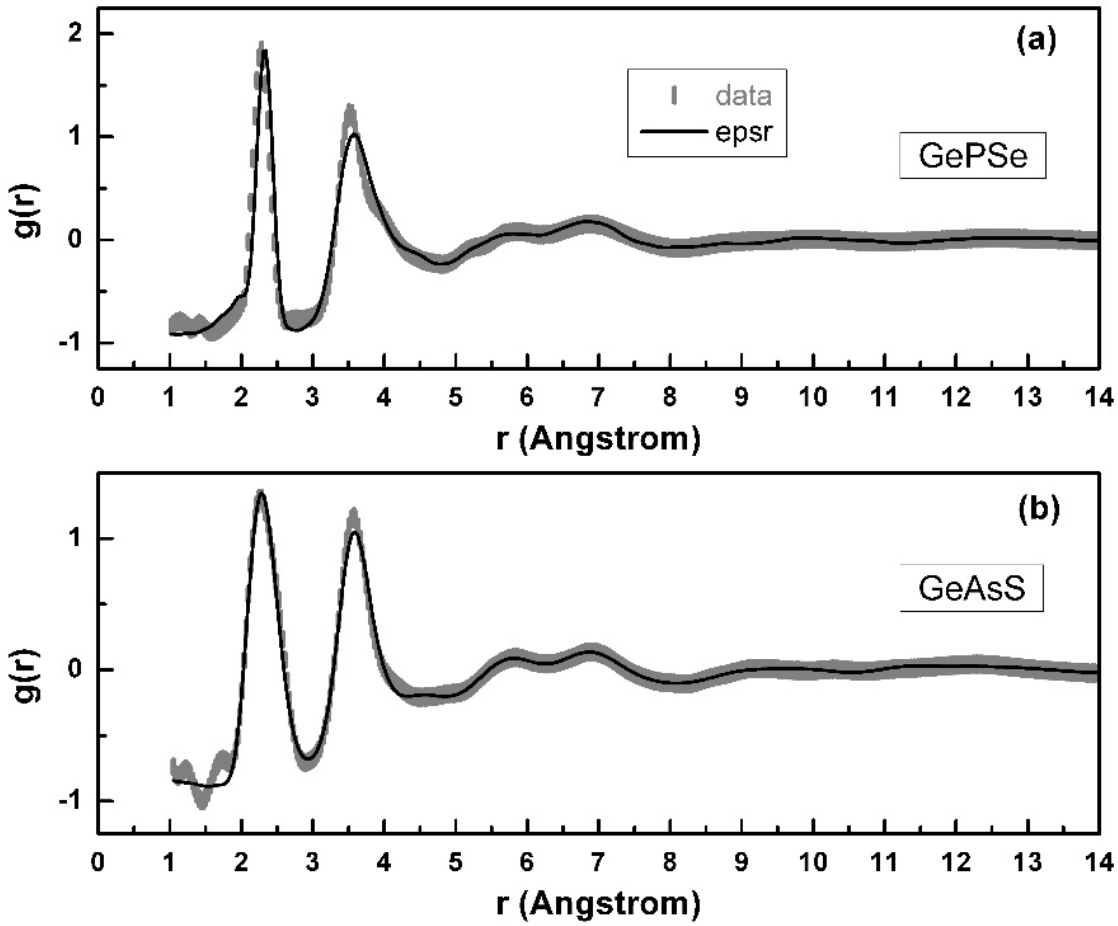


Figure 3. Total pair distribution functions, G(r), for (a) GPS and (b) GAS calculated from our EPSR simulations (solid black lines) compared with values calculated from our experimental data (gray thick bars).

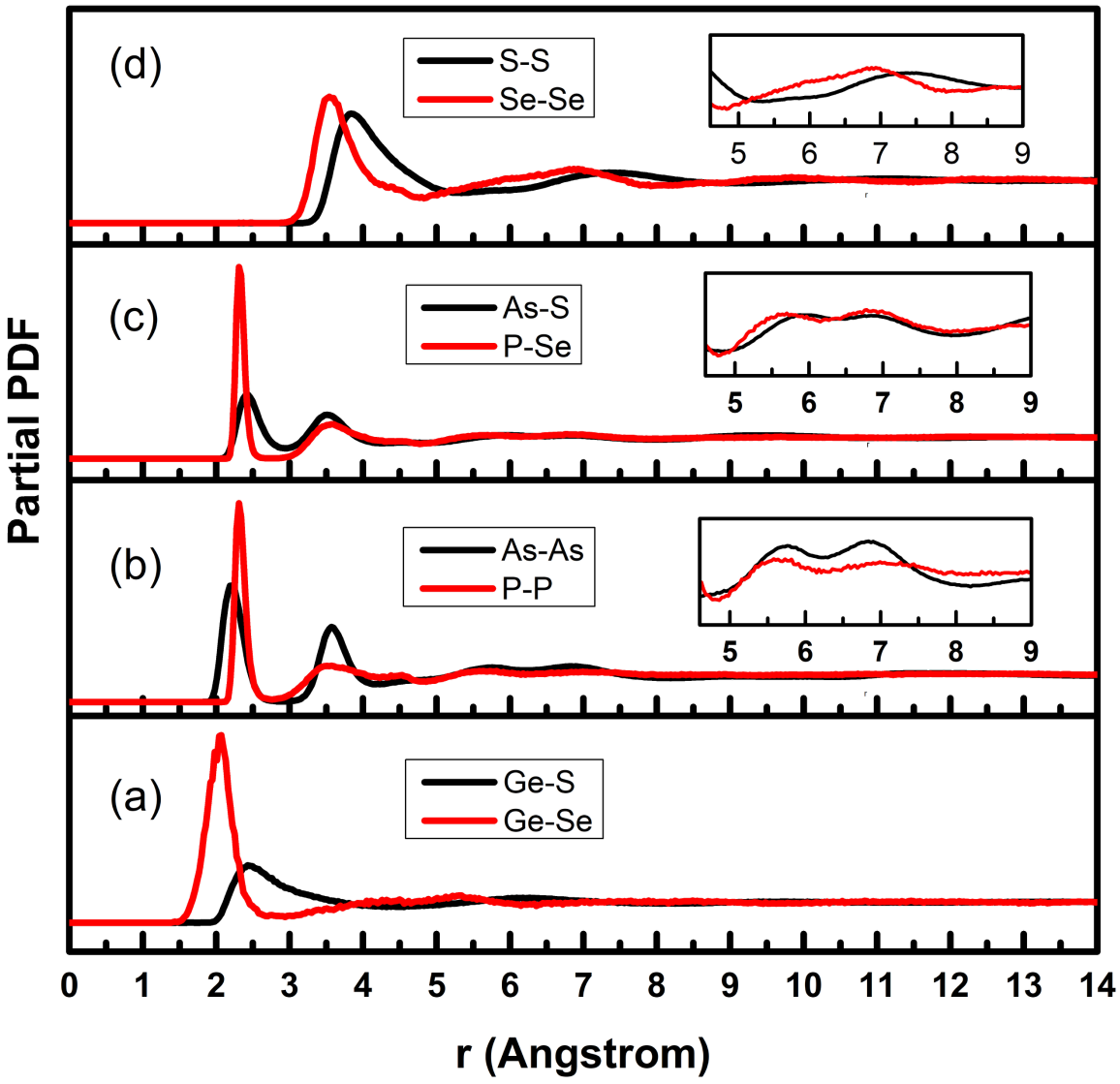


Figure 4. Partial pair distribution functions for: (a) Ge-Se and Ge-S, (b) P-P and As-As, (c) P-Se and As-S, and (d) Se-Se and S-S determined from the EPSR simulations.

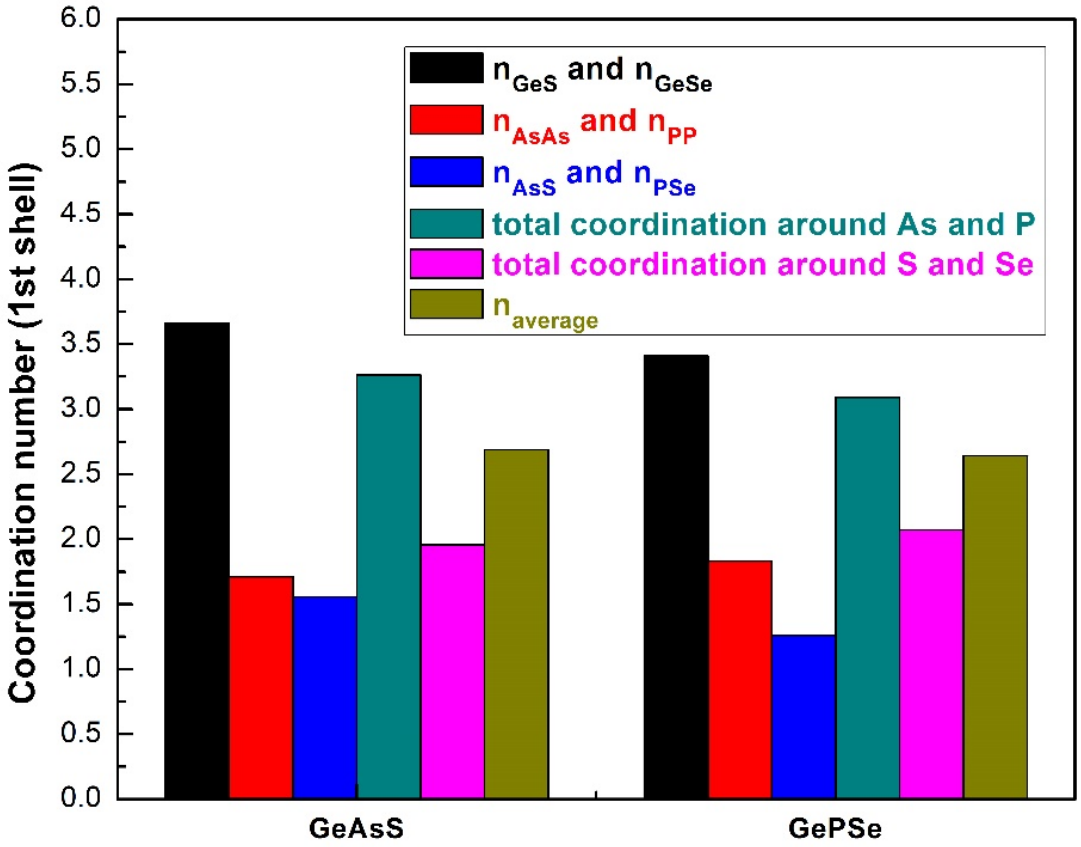


Figure 5. The nearest-neighbor coordination numbers calculated from our EPSR simulations.

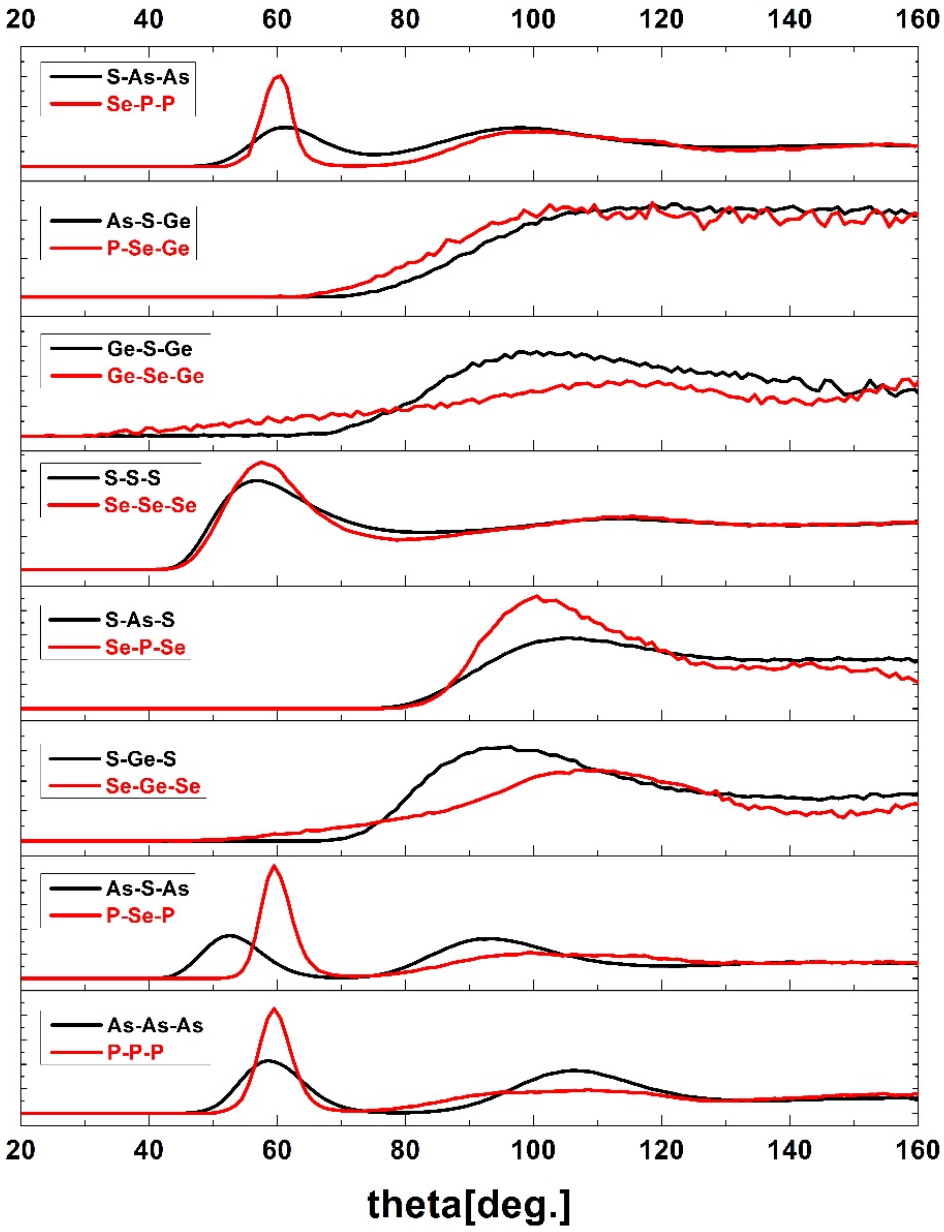


Figure 6. Bond angle distribution functions obtained from our EPSR simulations. All bond angle distribution functions, except the Se-Se-Se and S-S-S distributions, were calculated by including neighbors separated by less than 2.9 Å. For the Se-Se-Se and S-S-S distributions neighboring atoms are defined to be in the range of 2.5 Å < r < 4.5 Å.

| Bond-angle distribution | Peak position | Structural Motif |
|---|---|---|
| As-As-As | ~59°, ~107° | 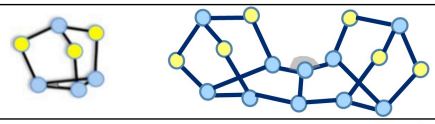 |
| P-P-P | ~60°, ~98° | 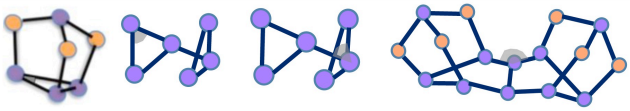 |
| As-S-As | ~52°, ~93° | 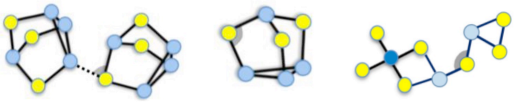 |
| P-Se-P | ~60°, ~102° |  |
| S-Ge-S (Se-Ge-Se) | ~93° (~109°) |  |
| S-As-S (Se-P-Se) | ~102° (~100°) | 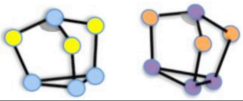 |
| S-S-S (Se-Se-Se) | ~58° (~59°) |  |
| Ge-S-Ge (Ge-Se-Ge) | ~99° (~112°) | 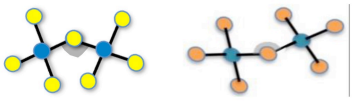 |
| S-As-As (Se-P-P) | ~61°, ~97° (~60°,~98°) | 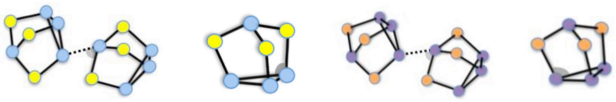 |


Figure 7. Structural motifs found in GAS and GPS together with their corresponding peaks in the bond angle distribution functions.

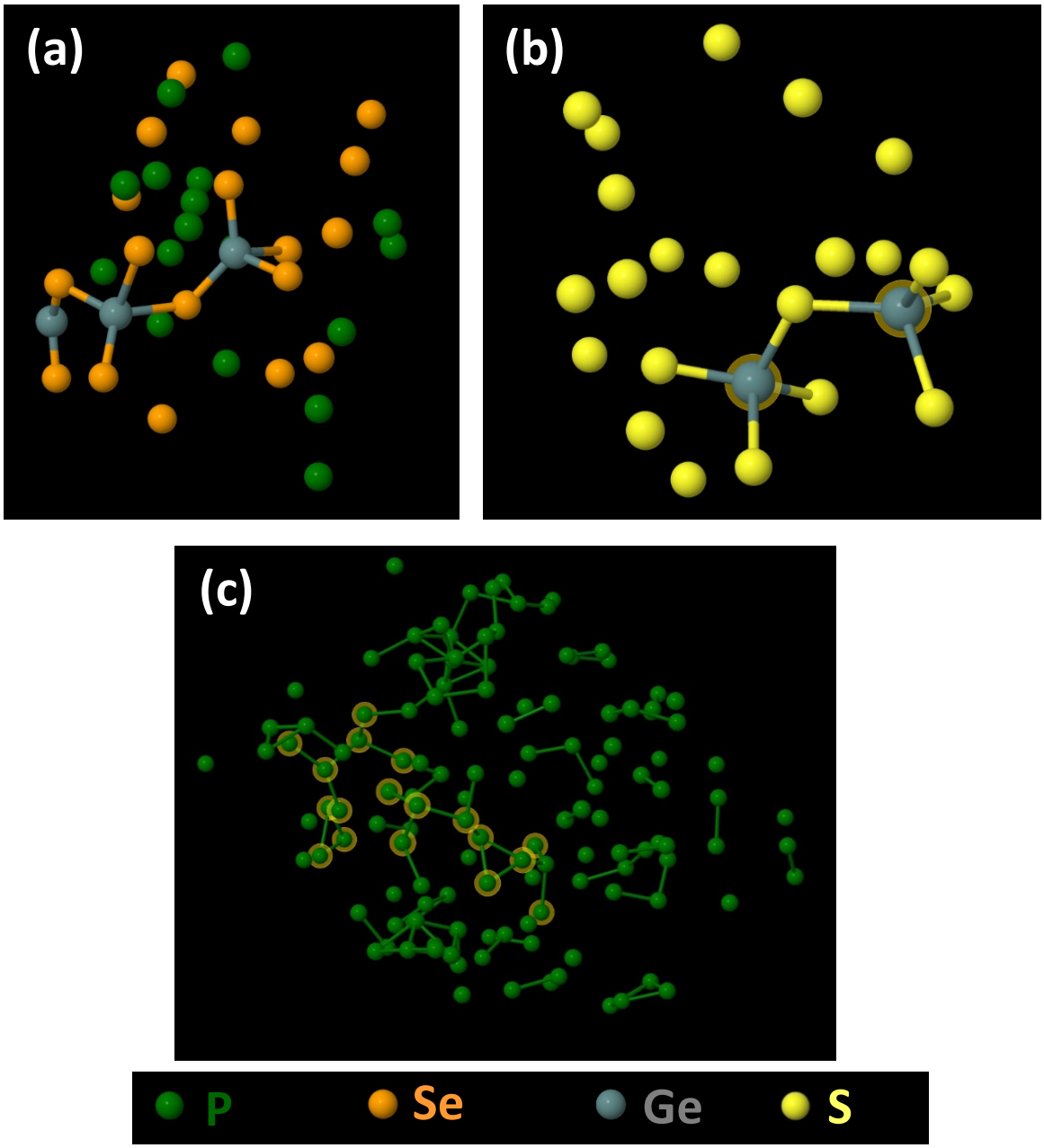


Figure 8. Structural motifs captured directly from the EPSR simulation boxs. (a) Corner-shared $GeSe_4$ tetrahedral units, (b) Corner-shared $GeS_4$ tetrahedral units, (c) Amorphous red-phosphorus type environments.

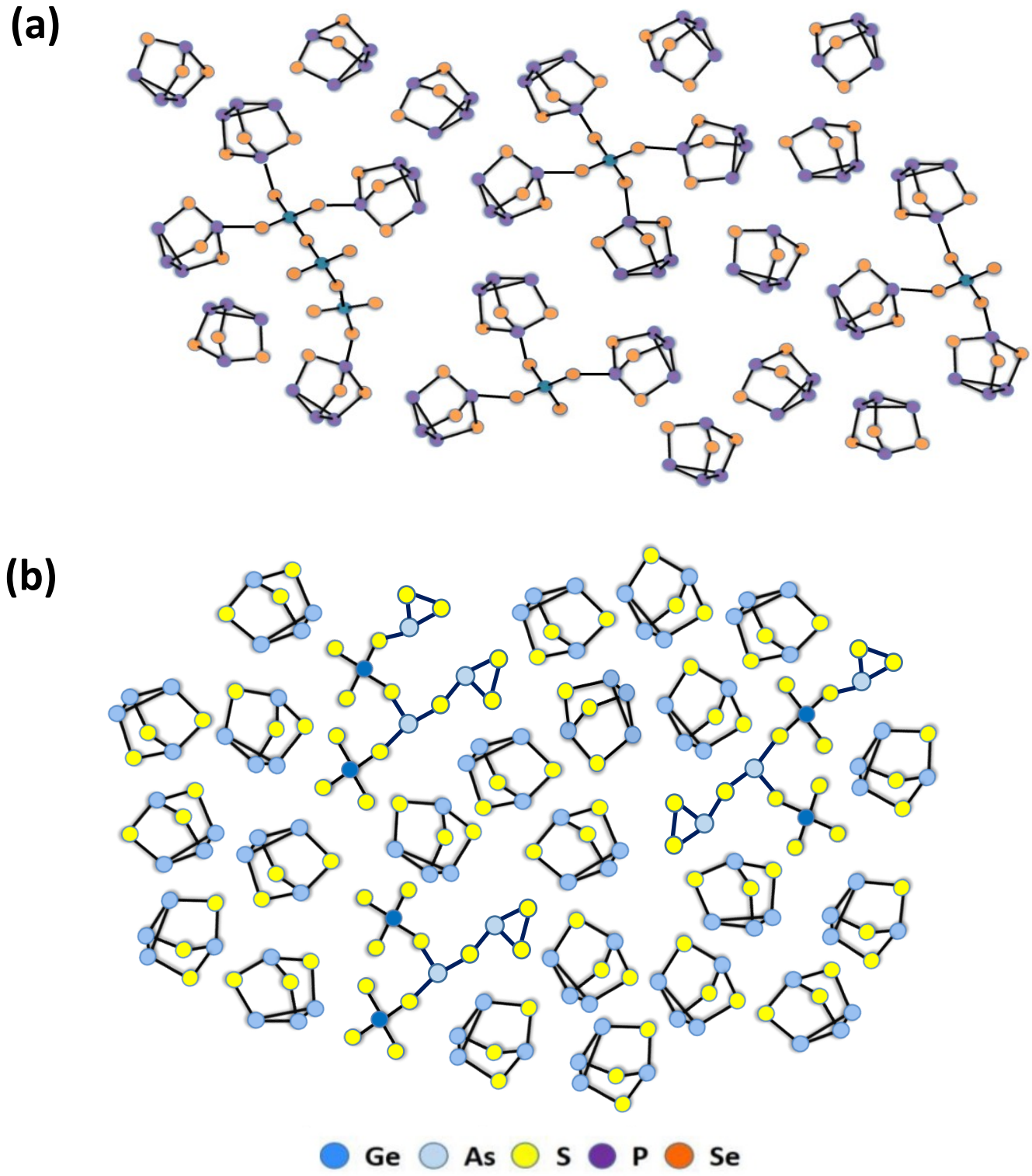


Figure 9. A schematic representation of the major structural components found in (a) GPS and (b) GAS glass. Their relative concentrations are only approximate.

Table 1. Mass and atomic number densities, and minimum approach distances used to build the simulation boxes for the EPSR simulations.

| Pairs | Minimum approach distances (Å) | Pairs | Minimum approach distances (Å) |
|---|---|---|---|
| Ge-Ge | 2.80 | Ge-Ge | 3.30 |
| Ge-Se | 1.60 | Ge-S | 1.60 |
| P-P | 2.16 | As-As | 1.95 |
| P-Se | 2.17 | As-S | 2.08 |
| Ge-P | 2.80 | Ge-As | 3.30 |
| Se-Se | 3.00 | S-S | 3.25 |
| Glass | Mass density ($g/cm^3$) | Atomic number density (atoms/ $Å^3$) | |
| GePSe | 3.09 | 0.0350 | |
| GeAsS | 3.35 | 0.0362 | |

Table 2. The number of atoms and Lennard-Jones parameters used in the EPSR models.

| Element | Number of atoms(GePSe) | Number of atoms(GeAsS) | Ɛ (kJ/mol) | σ (Å) |
|---|---|---|---|---|
| Ge | 56 | 50 | 0.10 | 2.00 |
| P | 1154 | - | 0.50 | 2.20 |
| Se | 790 | - | 0.10 | 2.00 |
| As | - | 1025 | 0.10 | 2.50 |
| S | - | 925 | 0.25 | 3.13 |